Available online at www.sciencedirect.com
ScienceDirect
Journal of Solid State Chemistry 179 (2006) 3467–3477
JOURNAL OF SOLID STATE CHEMISTRY
www.elsevier.com/locate/jssc

Subsolidus phase equilibria and properties in the system Bi_2O_3:$Mn_2O_{3\pm x}$:Nb_2O_5

T.A. Vanderah[a,*], M.W. Lufaso[a,1], A.U. Adler[a], I. Levin[a], J.C. Nino[b], V. Provenzano[a], P.K. Schenck[a]

[a]*National Institute of Standards and Technology, Materials Science and Engineering Laboratory, Gaithersburg, MD 20899, USA*
[b]*University of Florida, Department of Materials Science and Engineering, Gainesville, FL 32611-6400, USA*

Received 4 May 2006; received in revised form 5 July 2006; accepted 13 July 2006
Available online 16 July 2006

Abstract

Subsolidus phase relations have been determined for the Bi–Mn–Nb–O system in air (750–900 °C). Phases containing Mn^{2+}, Mn^{3+}, and Mn^{4+} were all observed. Ternary compound formation was limited to pyrochlore ($A_2B_2O_6O'$), which formed a substantial solid solution region at Bi-deficient stoichiometries (relative to $Bi_2(Mn,Nb)_2O_7$) suggesting that ≈14–30% of the A-sites are occupied by Mn (likely Mn^{2+}). X-ray powder diffraction data confirmed that all Bi–Mn–Nb–O pyrochlores form with structural displacements, as found for the analogous pyrochlores with Mn replaced by Zn, Fe, or Co. A structural refinement of the pyrochlore 0.4000:0.3000:0.3000 Bi_2O_3:$Mn_2O_{3\pm x}$:Nb_2O_5 using neutron powder diffraction data is reported with the A and O′ atoms displaced (0.36 and 0.33 Å, respectively) from ideal positions to 96g sites, and with Mn^{2+} on A-sites and Mn^{3+} on B-sites ($Bi_{1.6}Mn^{2+}_{0.4}(Mn^{3+}_{0.8}Nb_{1.2})O_7$, $Fd\bar{3}m$ (♯227), $a = 10.478(1)$ Å); evidence of A or O′ vacancies was not found. The displacive disorder is crystallographically analogous to that reported for $Bi_{1.5}Zn_{0.92}Nb_{1.5}O_{6.92}$, which has a similar concentration of small B-type ions on the A-sites. EELS spectra for this pyrochlore were consistent with an Mn oxidation between 2+ and 3+. Bi–Mn–Nb–O pyrochlores exhibited overall paramagnetic behavior with negative Curie–Weiss temperature intercepts, slight superparamagnetic effects, and depressed observed moments compared to high-spin, spin-only values. At 300 K and 1 MHz the relative dielectric permittivity of $Bi_{1.600}Mn_{1.200}Nb_{1.200}O_7$ was ≈128 with tan $\delta = 0.05$; however, at lower frequencies the sample was conductive which is consistent with the presence of mixed-valent Mn. Low-temperature dielectric relaxation such as that observed for $Bi_{1.5}Zn_{0.92}Nb_{1.5}O_{6.92}$ and other bismuth-based pyrochlores was not observed. Bi–Mn–Nb–O pyrochlores were readily obtained as single crystals and also as textured thin films using pulsed laser deposition.

Keywords: Pyrochlore; Displacive disorder; Bismuth manganese niobates; Bi–Mn–Nb–O; Phase equilibria; Phase diagram; Dielectric properties; Magnetic properties

1. Introduction

Considerable practical and fundamental interest exists in materials in which interactions occur between electric and magnetic dipoles; e.g., multiferroic materials, which exhibit the unusual coexistence of ferroelectricity and ferromagnetism as well as coupling between their order parameters [1–4]. So-called multifunctional magnetoelectric materials exhibit magnetic behavior that can be manipulated by electric fields, and vice versa [5,6]. Such materials, with high dielectric permittivity and high magnetic permeability, could serve as both inductors and capacitors in resonant circuits, and could enable entirely new applications such as multiple-state memory elements, electric-field-controlled ferromagnetic resonance devices, and transducers with magnetically modulated piezoelectricity [3,7–10]. The factors underlying the occurrence of these properties are not understood—only a few multiferroic compounds are known [3,11], including $BiMnO_3$ [12,13] and several other complex manganates [14–17]. Efforts continue to find new compounds [10,18] with robust, technically exploitable

*Corresponding author. Fax: +301 975 5334.
E-mail address: terrell.vanderah@nist.gov (T.A. Vanderah).
[1]Permanent address: University of North Florida, Department of Chemistry and Physics, Jacksonville, FL 32224.

0022-4596/$ - see front matter © 2006 Elsevier Inc. All rights reserved.
doi:10.1016/j.jssc.2006.07.014

magnetoelectric responses. The present study of the Bi_2O_3–$Mn_2O_{3\pm x}$–Nb_2O_5 system was undertaken to elucidate the phase equilibria of $BiMnO_3$ in the ternary system, and to reveal compound formation among strongly polarizable and magnetic cations.

2. Experimental methods

Fifty-two polycrystalline specimens (3–4 g each) were prepared in air by solid-state reactions using Bi_2O_3 (99.999%), "$MnCO_3$" (99.99%, pre-analyzed by thermogravimetric decomposition in air to Mn_3O_4), and Nb_2O_5 (99.999%). Prior to each heating, each sample was mixed by grinding with an agate mortar and pestle for 15 min, pelletized, and placed on a bed of sacrificial powder of the same composition supported on alumina ceramic. After an initial overnight calcine at 800 °C (below the m.p. of Bi_2O_3, 825 °C) multiple 1–3 d heatings (with intermediate grinding and re-pelletizing) were carried out at 885–900 °C.[2] Samples were furnace-cooled to ~700 °C and then air-quenched on the bench-top. Metastable melting in non-equilibrated ternary specimens, an initial problem owing to large differences in the melting points of Bi_2O_3, MnO_x, and Nb_2O_5, was avoided by soaking samples at 885 °C for 2–3 d for the second heating, followed by a third overnight heating at 900 °C. Equilibrium was presumed when no further changes could be detected in the weakest peaks observed in the X-ray powder diffraction patterns. A eutectic in the ternary system may occur near 50:25:25 Bi_2O_3:$Mn_2O_{3\pm x}$:Nb_2O_5, which formed liquid at 925 °C. Bi_2O_3 volatilization was observed above the solidus by thermogravimetric analysis, but was not detectable in the subsolidus study.

Pyrochlore-type crystals were easily obtained by heating a single-phase polycrystalline specimen (composition 40:30:30 Bi_2O_3:$Mn_2O_{3\pm x}$:Nb_2O_5) in a Pt capsule (sealed by welding) to 1300 °C, followed by slow cooling (5 °C/h) to below the freezing point (≈1175 °C). The crystals were obtained as brown-black shards and exhibited conchoidal fracture. The refined unit cell parameter obtained for a powdered sample of the crystals ($a = 10.495(1)$ Å) was larger than that of the starting material ($a = 10.478(1)$ Å), suggesting higher Bi-content in the crystals. Pyrochlore films were readily deposited by pulsed laser deposition (248 nm KrF EXCIMER, 10 Hz, 10 J/cm^2, background pressure 24 Pa O_2) from a target disk prepared by sintering (1050 °C, 8 h) single-phase pyrochlore powder (composition 40:30:30 Bi_2O_3:$Mn_2O_{3\pm x}$:Nb_2O_5). Films grew at high deposition rates (≈0.4 nm/s) on Si- and Pt-coated Si substrates. Crystalline, highly ⟨111⟩ textured films were obtained by either cold deposition in vacuum, followed by annealing for 10 min at 700 °C, or by deposition at 600 °C in 17 Pa O_2.

Phase assemblages were ascertained using the disappearing phase method [19,20] and X-ray powder diffraction data obtained with a Philips[3] diffractometer equipped with incident Soller slits, a θ-compensating slit and graphite monochromator, and a scintillation detector. Samples were mounted in welled glass slides. Patterns were collected at ambient temperatures using Cu$K\alpha$ radiation over the range 3–70° 2θ with a 0.02° 2θ step size and a 2 s count time. Intensity data measured as relative peak heights above background were obtained using the DATASCAN software package, and processed using JADE. For unit cell refinements, observed 2θ line positions were first corrected using SRM 660, LaB_6 [21], as an external calibrant. Lattice parameters were refined using JADE (2θ values, Cu$K\alpha_1$ = 1.540593 Å). Single pyrochlore-type crystals were characterized by the precession camera method (Zr-filtered Mo$K\alpha$ radiation) to assess quality, cell parameter, and space group.

Neutron powder diffraction data were collected using the BT-1 32-detector neutron powder diffractometer at the NIST Center for Neutron Research, NBSR. The specimen (10 g) was loaded in a vanadium container of length 50 mm and diameter 12.4 mm. A Cu(311) monochromator with a 90° take-off angle, $\lambda = 1.5402(2)$ Å, and in-pile collimation of 15 min of arc were used. Data were collected under ambient conditions and at 12 K, over the range of 3–168° 2θ with a step size of 0.05°. The instrument is described at the website http://www.ncnr.nist.gov/.

The oxidation state of Mn in selected samples was evaluated by electron energy loss spectroscopy (EELS) using polycrystalline specimens which were crushed in acetone and dispersed on lacey carbon-coated grids. EELS measurements of the Mn–$L_{2,3}$ edge were conducted in a JEOL-3010 UHR (300 kV) transmission electron microscope (TEM) equipped with a LaB_6 electron source, Gatan Imaging Filter (GIF), and a slow-scan charge-coupled device (CCD) camera. The EELS spectra were recorded with the TEM operated in the diffraction mode using a 0.6 mm GIF entrance aperture, energy dispersion of 0.1 eV/channel, and 30 s integration time (under the chosen conditions, the full-width at half-maximum of the zero-loss peak was 1.7 eV). Mn_3O_4 ($Mn^{3+/2+}$) and $MnNb_2O_6$ (Mn^{2+}) were analyzed as reference samples. For each sample, 10 spectra were collected from distinct particulates. The averaged background-subtracted spectra were processed to remove the effect of plural inelastic scattering using a Fourier-ratio deconvolution method [22]. Since all spectra were collected from sufficiently thin areas, the effect of this deconvolution was rather small.

[2]Exceptions: specimens with Bi contents >70 mol% were not heated above 750 °C (to avoid melting and decomposition of sillenite-type phases), and those with Bi contents ⩽20 mol% were heated at higher final temperatures, 975–1200 °C, to achieve equilibrium more quickly.

[3]Certain commercial equipment and software are identified in order to adequately specify the experimental procedure; recommendation or endorsement by the National Institute of Standards and Technology is not therein implied.

Magnetic properties were characterized using a Quantum Design SQUID magnetometer and single-phase polycrystalline samples. Magnetization was measured as a function of temperature between 2 and 300 K after cooling in the absence of an applied field (zero-field cooled, ZFC) and after cooling in a magnetic field (field-cooled, FC) of 50 kG. In addition, measurements at 4.2 K and at ambient temperature were carried out to determine the field dependence of the magnetization in applied fields between 0 and 50 kG.

Dielectric properties were evaluated using sintered (1050 °C, 4 h) pellets (≈13 mm diameter, ≈1 mm thick) of single-phase specimens which were polished to obtain planar surfaces. Density was determined geometrically. Gold electrodes (≈75 nm thick) were sputtered onto the pellet surfaces to form parallel plate capacitors. Capacitance and dielectric loss were measured using an Agilent 4284 LCR meter at frequencies varying from 10 kHz to 1 MHz. Reported permittivity data have been corrected to theoretical density. Although the sample temperature was varied between 110 and 450 K using a programmable 9023 Delta Design controller, data is reported only up to 300 K due to the high conductivity observed. Typical uncertainties in the permittivity data are on the order of 5% and are dominated by the geometric estimates of porosity.

3. Results and discussion

3.1. Phase formation

The results of the phase equilibrium study are presented in Fig. 1. Previously reported diagrams for the binary perimeter systems [23] were mostly confirmed in the present study. In the Mn–Nb–O system only the Mn^{2+} compound manganocolumbite, $MnNb_2O_6$, was observed to form. In the Bi–Mn–O system two compounds formed, sillenite-type $Bi_{12}MnO_{20}$ (Mn^{4+}) [24] and $Bi_2Mn_4O_{10}$, which contains ordered Mn^{3+} and Mn^{4+} in pyramidal and octahedral coordination, respectively [25,26]. The high-pressure (3–6 GPa/700 °C) perovskite-related $BiMnO_3$ phase [27–29] was not observed in the study of the ternary system; this compound decomposes at 600 °C when heated under ambient pressure [30], and was not stabilized in the presence of Nb_2O_5. The binary Bi–Nb–O phases observed were in general agreement with the comprehensive study reported by Roth [31] except for the high-Bi_2O_3 (⩾0.75 mol fraction) region, represented in Fig. 1 as a "fluorite" solid solution extending from 75:25 Bi_2O_3:Nb_2O_5 ($Bi_3Nb_2O_7$) to 93:7 Bi_2O_3:Nb_2O_5 and dissolving ~2 mol% $Mn_2O_{3\pm x}$, as shown. This region of the Bi_2O_3:Nb_2O_5 system has received considerable attention as it forms a series of structurally complex, modulated

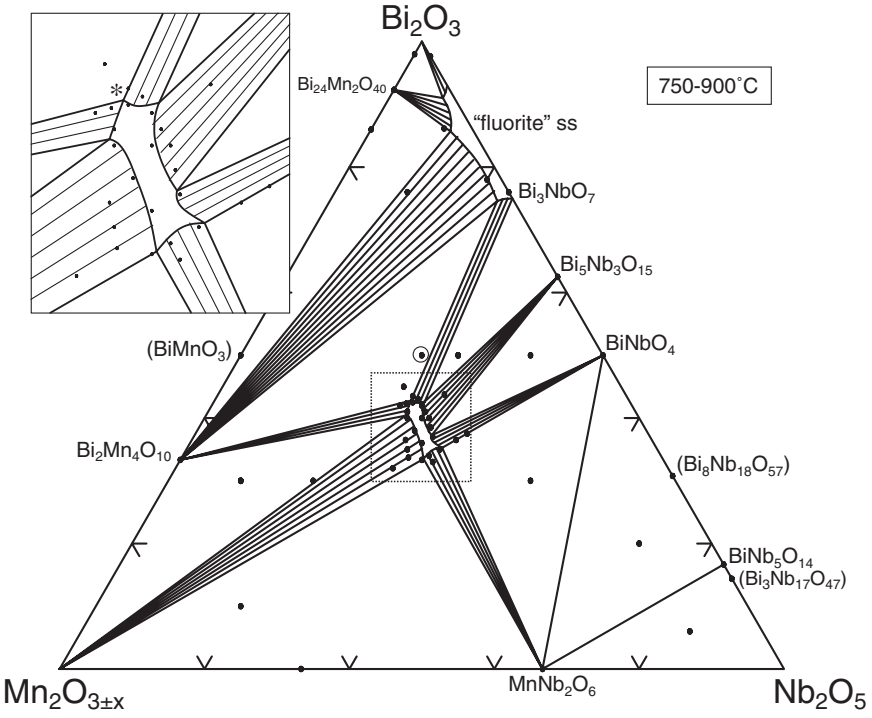

Fig. 1. Subsolidus phase equilibrium diagram in air for the Bi_2O_3:$Mn_2O_{3\pm x}$:Nb_2O_5 system. Black dots denote the compositions of specimens prepared in the study; concentrations are on a molar fraction basis. Ternary phase formation is limited to pyrochlore, which forms an appreciable solid solution near the center of the diagram (enlarged in the inset). The "pyrochlore-like" composition Bi_2MnNbO_7 (open circle) is not included in the solid-solution region, but rather forms a three-phase mixture of Bi_3NbO_7 solid solution, pyrochlore, and $Bi_2Mn_4O_{10}$. The limiting compositions of the pyrochlore field suggested by the present data are (inset: clockwise beginning with the cusp marked with an asterisk) Bi_2O_3 : $Mn_2O_{3\pm x}$:Nb_2O_5 = 0.429:0.302:0.269 ($Bi_{1.70}Mn_{1.20}Nb_{1.06}O_{7-x}$, a = 10.484(1) Å), 0.428:0.282:0.290 ($Bi_{1.67}Mn_{1.10}Nb_{1.13}O_{7-x}$, a = 10.516(1) Å), 0.377:0.298:0.325 ($Bi_{1.45}Mn_{1.14}Nb_{1.25}O_{7-x}$, a = 10.478(1) Å), 0.352:0.297:0.351 ($Bi_{1.33}Mn_{1.12}Nb_{1.33}O_{7-x}$, a = 10.461(1) Å), 0.333:0.330:0.337 ($Bi_{1.27}Mn_{1.26}Nb_{1.28}O_{7-x}$, a = 10.439(1) Å), and 0.404:0.320:0.276 ($Bi_{1.59}Mn_{1.26}Nb_{1.09}O_{7-x}$, a = 10.462(1) Å) (x = 0 corresponds to all Mn^{3+}).

superstructures [32–36] with variable and potentially useful dielectric properties [33,37–39]. Reported differences in the detailed phase relations in this region likely arise from kinetic effects, variations in synthesis (especially cooling methods), and/or differences in characterization methods (e.g., X-ray or electron diffraction). For example, the present study, in agreement with early studies [31], did not find a sillenite-type compound at the composition $Bi_{12}Nb_{0.29}O_{20-x}$ [33]. This specimen was a mixture of monoclinic Bi_2O_3 and the fluorite-type solid solution after repeated heatings at 700 °C for a total of 414 h; however, a different heat treatment may have resulted in the metastable body-centered cubic form of Bi_2O_3 (sillenite-type) [40] instead of the monoclinic polymorph.

Ternary phase formation in the Bi_2O_3:$Mn_2O_{3\pm x}$:Nb_2O_5 system was found to be limited to pyrochlore, which forms an appreciable solid solution region (Fig. 1). During synthesis, the pyrochlore phase formed early in partially reacted samples and was readily purified within the single-phase region, suggesting high thermodynamic stability. Numerous descriptions can be found for the pyrochlore crystal structure, $^{VIII}A_2^{VI}B_2O_7$, which is unusual in that it can be considered as two relatively independent interpenetrating networks: [BO_6] octahedra sharing all vertices, and [$O'A_4$] tetrahedra in an anti-cristobalite-type arrangement [41–44]. The structural formula is often written as $(A_2O')(B_2O_6)$ or $A_2B_2O_6O'$ to emphasize this interesting structural character. The larger A-cations are 8-fold ($=6+2$) coordinated by six oxygens in puckered rings formed by the B_2O_6 network plus two O' oxygens above and below in the A_2O' network. The structure inherently facilitates non-stoichiometry as the A_2O' network can be partially occupied, or in some cases completely absent; furthermore, numerous non-oxide and halide pyrochlores are known. In addition to extensive compositional ranges, pyrochlores exhibit a remarkable variety of exploitable physical properties, hence the considerable technical importance of this class of solids [43,45–47].

Bi–Mn–Nb–O pyrochlores have been previously reported to form at the stoichiometries $Bi_2Mn_2Nb_2O_{11+y}$, $Bi_2Mn_3Nb_2O_{11+y}$ [48], Bi_2MnNbO_7 [49], and $Bi_{1.5}MnNb_{1.5}O_7$ [50]; however, under the conditions of the present study none of these compositions fall in the pyrochlore single-phase field: Composition $Bi_2Mn_2Nb_2O_{11+y}$ formed mostly pyrochlore with a small amount of Mn_2O_3, $Bi_2Mn_3Nb_2O_{11+y}$ falls in a two-phase region of pyrochlore and a considerable amount of Mn_2O_3/Mn_3O_4, Bi_2MnNbO_7 formed a three-phase mixture as described in Fig. 1, and $Bi_{1.5}MnNb_{1.5}O_7$ formed a mixture of pyrochlore and $BiNbO_4$. As shown on the diagram (Fig. 1), Bi–Mn–Nb–O pyrochlores form thermodynamically stable mixtures with the Bi_3NbO_7 solid solution, $Bi_5Nb_3O_{15}$, $BiNbO_4$, $MnNb_2O_6$, Mn_2O_3/Mn_3O_4, and $Bi_2Mn_4O_{10}$. Compositions, nominal formulas, and refined unit cell parameters for single-phase Bi–Mn–Nb–O pyrochlores prepared in the present study are given in Table 1; all specimens were black in color. The trends in unit cell parameters suggest that cell volume increases markedly with both Bi and vacancy concentration.

Table 1
Compositions, nominal formulas, and refined unit cell parameters (*a*, space group $Fd\bar{3}m$, #227) for single-phase pyrochlore specimens prepared in this study

Bi_2O_3:$Mn_2O_{3\pm x}$:Nb_2O_5	Nominal Formula (Mn^{3+})	*a* (Å)
0.4250:0.3000:0.2750	$Bi_{1.676}\square_{0.056}Mn_{1.183}Nb_{1.084}O_{7-x}$	10.482(1)
0.4200:0.2900:0.2900	$Bi_{1.642}\square_{0.089}Mn_{1.134}Nb_{1.134}O_{7-x}$	10.499(1)
0.4100:0.3150:0.2750	$Bi_{1.617}\square_{0.056}Mn_{1.242}Nb_{1.084}O_{7-x}$	10.466(1)
0.4000:0.3000:0.3000	$Bi_{1.556}\square_{0.111}Mn_{1.167}Nb_{1.167}O_{7-x}$	10.478(1)
0.3600:0.3200:0.3200	$Bi_{1.385}\square_{0.154}Mn_{1.231}Nb_{1.231}O_{7-x}$	10.451(1)

These compositions correspond to the points within the six-sided pyrochlore region shown in Fig. 1. For purposes of comparison, the formulas have been normalized to seven oxygens (full occupancy of the O′ site) and assume Mn^{3+} ($x=0$). Although the metal ratios given here are precise, the actual populations on the A and B sites depend on the O′ occupancy factor and Mn oxidation state(s), which are uncertain and which may vary in each pyrochlore.

Observed, indexed X-ray powder diffraction data for the pyrochlore 0.4000:0.3000:0.3000 Bi_2O_3:$Mn_2O_{3\pm x}$:Nb_2O_5 are given in Table 2. As noted previously [43], the 442 reflection, forbidden for an ideal pyrochlore structure, was readily observed in this pattern and in all patterns of pyrochlore and pyrochlore-containing specimens prepared in this study. The 442 reflection was also observed in precession photos of single crystals. Similar to the Bi–Zn–Nb–O pyrochlores [43,51], the presence of this diagnostic reflection indicates the presence of displacements off ideal crystallographic sites. The consistent observation of this reflection indicates that all Bi–M–Nb–O pyrochlores exhibit site displacements (either static or dynamic). Furthermore, the stoichiometric location of the pyrochlore phase field, as also found for the analogous Bi–M–Nb–O systems ($M=$ Zn [43], Fe [52], Co [53], occurs at substantially lower Bi concentrations than conventional formulations placing only Bi on the A-sites and the smaller M/Nb cations on the B-sites. The pyrochlore field includes compositions with "excess" B-cations that require mixing of some Mn on the A-sites with Bi^{3+}, as found for Zn in all Bi–Zn–Nb–O pyrochlores [43]. The limiting compositions observed for the pyrochlore field (Fig. 1) suggest that the Mn concentration on the A-sites can range from ≈14 to 30%[4]—higher levels than those observed for $M=$ Zn (≈16–26%) [43], Fe (≈4–15%) [52], or Co (≈8–25%) [53] in analogous Bi–M–Nb–O pyrochlores.

[4]Estimated by assuming an average Mn oxidation state of 2.75+ and full occupancy of the O′ site; the latter assumption results in maximum estimates for $Mn_{A\text{-site}}$ concentrations and minimum estimates for *A*-site vacancy concentrations.

Table 2
Observed X-ray powder diffraction data for pyrochlore-like 0.4000:0.3000:0.3000 Bi_2O_3:$Mn_2O_{3\pm x}$:Nb_2O_5 (space group $Fd\bar{3}m$, #227, $a = 10.478(1)$ Å)

h	k	l	$2\theta_{obs}$	I_{obs}	$2\theta_{calc}$	$\Delta 2\theta$	d_{obs}
1	1	1	14.640	5	14.631	0.009	6.0458
2	2	0	24.005	<1	24.003	0.002	3.7042
3	1	1	28.236	6	28.225	0.011	3.1580
2	2	2	29.515	100	29.508	0.008	3.0240
4	0	0	34.215	36	34.203	0.012	2.6186
3	3	1	37.380	10	37.380	0.000	2.4038
4	2	2	42.231	<1	42.219	0.012	2.1382
3	3	3	44.917	3	44.915	0.002	2.0164
4	4	0	49.148	47	49.148	0.000	1.8523
5	3	1	51.572	3	51.561	0.011	1.7708
4	4	2	52.338	<1	52.347	−0.010	1.7466
6	2	0	55.418	1	55.415	0.004	1.6566
5	3	3	57.636	<1	57.642	−0.006	1.5980
6	2	2	58.369	40	58.372	−0.004	1.5797
4	4	4	61.242	10	61.239	0.003	1.5123
7	1	1	63.340	1	63.338	0.003	1.4672
6	4	2	66.746	<1	66.753	−0.007	1.4003
5	5	3	68.749	<1	68.761	−0.012	1.3643

3.2. Oxidation state of Mn

In the present study conducted in air, compounds with di-, tri-, and tetravalent Mn were all obtained[5]; e.g., light tan $MnNb_2O_6$ (Mn^{2+}), black $Bi_{12}MnO_{20}$ (Mn^{4+}), and black $Bi_2Mn_4O_{10}$ ($Mn^{3+/4+}$). Both Mn_2O_3 (Mn^{3+}, bixbyite) and Mn_3O_4 ($Mn^{2+/3+}$, hausmannite) were observed in equilibrated mixtures prepared in the phase diagram study (MnO was not observed). The oxidation state of Mn in the pyrochlore phase $Bi_{1.556}Mn_{1.167}Nb_{1.167}O_{7-x}$ (Bi_2O_3:$Mn_2O_{3\pm x}$:$Nb_2O_5 = 0.4000 : 0.3000 : 0.3000$) was inferred from the observed relative intensities of the L_3 and L_2 lines in the EELS spectra. For transition metals with partially occupied 3d states, these so-called "white" lines arise from $2p^{3/2} \rightarrow 3d^{3/2}3d^{5/2}$ and $2p^{1/2} \rightarrow 3d^{3/2}$ transitions, and their intensities reflect the densities of unoccupied states in the 3d bands [54]. Systematic EELS studies have established a clear correlation between the white line intensities and the valence state of the 3d transition metals [55,56]. In particular, the L_3/L_2 ratio for Mn was observed to increase dramatically with a decrease in Mn valence from 4 to 2 [56]. Comparison of the Mn–$L_{2,3}$ spectra (Fig. 2) recorded from the pyrochlore sample to those for Mn_3O_4 ($Mn^{2+}/Mn^{3+} = 0.5$) and $MnNb_2O_6$ (Mn^{2+}) suggests that the valence of Mn is between 2+ and 3+ in the pyrochlore phase. Linear interpolation of the L_3/L_2 intensity ratios between the corresponding values for Mn_3O_4 and $MnNb_2O_6$ yields a valence state of ~2.2 for the Mn in the pyrochlore phase (a double-step background function was used to extract the L_3 and L_2 intensities, as described in Ref. [56]). This value is considered approximate since the coordination environment of Mn in the pyrochlore A-sites is expected to be considerably different from that in the reference compounds. Overall, the EELS results and the deep black colors of the Bi–Mn–Nb–O pyrochlores are both consistent with the presence of mixed-valent 2+/3+ Mn.

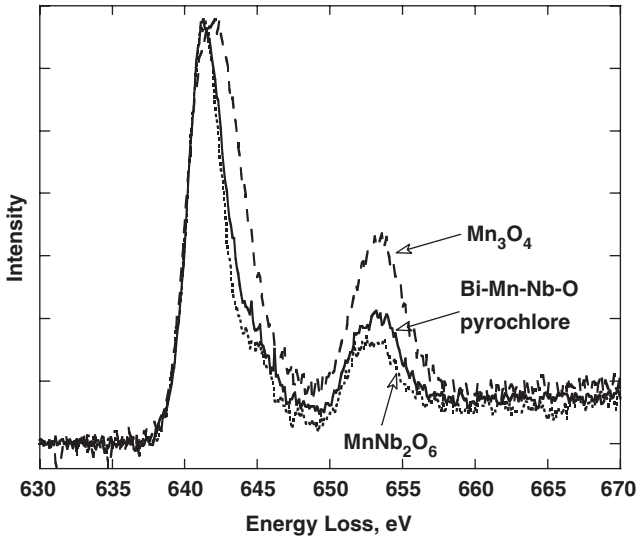

Fig. 2. Mn–$L_{2,3}$ edge in the EELS spectra observed for the pyrochlore phase $Bi_2O_3 : Mn_2O_{3\pm x}: Nb_2O_5 = 0.4000 : 0.3000 : 0.3000$ and reference samples Mn_3O_4 ($Mn^{2+/3+}$) and $MnNb_2O_6$ (Mn^{2+}). The similarity of the $L_{2,3}$ intensities for the pyrochlore and $MnNb_2O_6$ samples suggests that the average oxidation state of Mn in the pyrochlore is between 2+ and 3+.

3.3. Structural refinement of the pyrochlore phase

The highly symmetrical ideal pyrochlore structure $A_2B_2O_6O'$ crystallizes in space group $Fd\bar{3}m$ with A and B cations on two special positions (16d, 16c) and oxygens on two sites, 48f (O) and 8b (O′), resulting in a single positional variable (x for the 48f site oxygens in the B_2O_6 octahedral network). As expected, this model resulted in anomalously large thermal parameters for the A-site cations and the O′ oxygens in an initial refinement using neutron powder diffraction data collected from a single-phase pyrochlore sample, composition 0.4000:0.3000:0.3000 Bi_2O_3:$Mn_2O_{3\pm x}$:Nb_2O_5. Displacive disorder in the A_2O' network has been reported for numerous pyrochlores [43]. For $Bi_{2-x}M_xRu_2O_{7-y}$ (M = Cu, Co; $x = 0$; 0:4), the disorder was attributed to the lone pairs on Bi^{3+} [57]. Pyrochlores in the $Sn^{2+}_{2-x}(M_{2-y}Sn^{4+}_y)O_{7-x-y/2}$ (M = Nb^{5+} or Ta^{5+}) series were found to have both cation and anion vacancies as well as static displacements of O′ [58]. Static disorder has also been reported for the defect pyrochlores $Tl_2Nb_2O_6$ and $Tl_2Ta_2O_6$ [59,60], $Bi_2Ti_2O_7$ [61], $Bi_{2-x}CrTaO_{7-y}$ [62], and $Bi_2Sn_2O_7$ [63,64]. Another study of $Tl_2Nb_2O_{6+x}$ phases concluded that, in agreement with NMR results, the forbidden reflections were better accounted for by anisotropic thermal (rather than static) displacements [65].

[5]The four-component system actually studied, Bi_2O_3–MnO–MnO_2–Nb_2O_5, is represented for simplicity as a projection on a ternary slice (Fig. 1).

Various models have been used to refine the structures of displacively disordered pyrochlores. In an X-ray single-crystal diffraction study of $Tl_2Ta_2O_6$, Tl^+ ions were displaced from the 16d to the 32e sites, yielding two equivalent half-occupied positions [60]. For $Bi_{2-y}Ru_2O_{7-z}$ [57], $Bi_{2-y}Yb_yRu_2O_{7-z}$ [60], and $Bi_{2-x}CrTaO_{7-y}$[62], Bi was displaced to the 96 h site, yielding a toroid of six possible equivalent positions. In the structural refinement of $Bi_{1.5}Zn_{0.92}Nb_{1.5}O_{6.92}$ [51] both the A cations and O′ oxygens were displaced to 96g sites, resulting in six equivalent possible positions for the former and 12 for the latter; a study of short-range ordering has also been reported for this pyrochlore [66]. For $Bi_{2-y}Ru_2O_{7-z}$ [57] the O′ oxygens were displaced from the 8b to the 32e site, distributed among four equivalent positions. Although the displacively disordered sites in the different models are crystallographically distinct, the refinements in general indicate similar magnitudes for the displacements of A and O′ from the ideal positions (on the order of $\leqslant 0.5$ Å).

Rietveld refinement results obtained for pyrochlore-type 0.4000:0.3000:0.3000 Bi_2O_3:$Mn_2O_{3\pm x}$:Nb_2O_5 using five different models and neutron powder diffraction data are given in Table 3. Cation ratios were fixed according to the preparative analytical masses; no impurity phases were detectable by X-ray or neutron diffraction; however, the oxidation state of Mn was uncertain. Two approaches were tried, the first assumed the presence of only Mn^{3+} ($Bi_{1.556}Mn^{3+}_{0.333}(Mn^{3+}_{0.833}Nb_{1.167})O_7$) and the second placed larger Mn^{2+} on the A-site and smaller Mn^{3+} on the B-site ($Bi_{1.6}Mn^{2+}_{0.4}(Mn^{3+}_{0.8}Nb_{1.2})O_7$); in both cases, the B- and O′-sites were assumed to be fully occupied. In all initial refinements, the composition with mixed $Mn^{2+/3+}$ gave better fits, as found in other neutron powder diffraction studies of Mn-containing pyrochlores which found high-spin Mn^{2+} on the A-site [67] and high-spin Mn^{3+} on the B-site [68]. Cation occupancies were therefore fixed according to the formula $Bi_{1.6}Mn^{2+}_{0.4}(Mn^{3+}_{0.8}Nb_{1.2})O_7$. The anomalously large thermal parameters obtained for the A- and O′- sites in Model 1 (ideal pyrochlore structure), when combined with the observation of 442-type reflections in the powder diffraction patterns, confirm the presence of displacements. In Models 2 and 3 the A-site cations were displaced onto the 96h and 96g sites, respectively, resulting in substantially improved fits and slightly better fit statistics for Model 3; however, the O′ thermal parameters remained large. Models 4 and 5 retained A-site cations on the 96g sites and displaced O′ to the 32e ((x, x, x) with $x\sim0.36$) or 96g ((x, x, z) with $x\sim0.35$ and $z\sim0.37$) sites, respectively. These models returned similar fit statistics, but the smaller O′ thermal parameter obtained with Model 5 suggests that its position is best described on the 96g site.

Final refinement results for pyrochlore-type 0.4000:0.3000:0.3000 Bi_2O_3:$Mn_2O_{3\pm x}$:Nb_2O_5 at 12 K and 293 K using Model 5 are given in Table 4; the difference profiles are shown in Fig. 3. The similar results obtained at the two temperatures suggest that the displacements are static in nature. The site occupancy obtained for O′ does not differ significantly from the fully occupied value of 1/12

Table 3
Refined structural parameters for pyrochlore-type 0.4000:0.3000:0.3000 Bi_2O_3:$Mn_2O_{3\pm x}$:Nb_2O_5 at ambient temperature using neutron powder diffraction data, space group $Fd\bar{3}m$ (♯227)

	Model 1	Model 2	Model 3	Model 4	Model 5
a (Å)	10.4761(1)	10.47617(9)	10.4761(1)	10.47615(8)	10.47615(8)
A-site	16d	96h	96g	96g	96g
Occ. (Bi, Mn)	0.8, 0.2	0.133, 0.033	0.133, 0.033	0.133, 0.033	0.133, 0.033
x (Bi, Mn)	1/2	0	0.4679(4)	0.4686(6)	0.4682(4)
y (Bi, Mn)	1/2	0.2264(1)	0.5094(3)	0.5098(4)	0.5095(4)
z (Bi, Mn)	1/2	0.7736(1)	0.5094(3)	0.5098(4)	0.5095(4)
U_{iso} (Bi, Mn) (Å^2) × 100	6.91(9)	1.69(6)	1.16(9)	1.32(10)	1.23(11)
B-site	16c	16c	16c	16c	16c
Occ. (Mn, Nb)	0.4, 0.6	0.4, 0.6	0.4, 0.6	0.4, 0.6	0.4, 0.6
U_{iso} (Mn, Nb) (Å^2) × 100	1.89(7)	1.94(5)	1.90(5)	1.90(5)	1.89(5)
O-site	48f	48f	48f	48f	48f
x (O)	0.3205(1)	0.32055(7)	0.32046(7)	0.32037(7)	0.32038(7)
U_{iso} (O) (Å^2) × 100	2.51(2)	2.35(2)	2.33(2)	2.33(2)	2.32(2)
O′-site	8b	8b	8b	32e	96 g
Occ. (O)	1	1	1	0.25	0.0833
x (O)	3/8	3/8	3/8	0.3597(5)	0.354(1)
y (O)	3/8	3/8	3/8	0.3597(5)	0.354(1)
z (O)	3/8	3/8	3/8	0.3597(5)	0.369(2)
U_{iso} (O) (Å^2) × 100	6.0(1)	6.49(9)	6.56(9)	3.5(2)	2.6(5)
R_{wp} (%)	6.09	4.31	4.26	4.23	4.22
R_p (%)	4.57	3.50	3.47	3.45	3.45
χ^2	2.66	1.328	1.302	1.279	1.278

Atoms retained on special positions in all models are B-site Mn/Nb on 16c (0, 0, 0) and oxygen on 48f (x, 0, 0).

Table 4
Final Rietveld refinement results for pyrochlore-type 0.4000:0.3000:0.3000 Bi_2O_3:$Mn_2O_{3\pm x}$:Nb_2O_5 using Model 5 (space group $Fd\bar{3}m$, #227) and neutron powder diffraction data

Name	x	y	z	U_i/U_e (Å^2) × 100	Site	Occ.
Bi/Mn	0.4723(6)	0.5145(6)	0.5145(6)	1.39(6)	96g	0.1333/0.0333
	0.4718(7)	0.5135(7)	0.5135(7)	1.69(6)	96g	0.1333/0.0333
Nb/Mn	0	0	0	1.77(5)	16c	0.6/0.4
	0	0	0	1.98(5)	16c	0.6/0.4
O	0.32034(7)	0.125	0.125	2.10*	48f	1
	0.32068(7)	0.125	0.125	2.39**	48f	1
O′	0.3641(8)	0.3641(8)	0.3777(16)	2.2(4)	96g	0.081(1)
	0.356(2)	0.356(2)	0.371(3)	3.4(7)	96g	0.082(1)

The upper and lower entries correspond to 12 and 293 K, respectively. The lattice parameter, cell volume, and final fit statistics at 12 K (293 K) are $a = 10.47242(8)$ Å (10.47616(8) Å), volume = 1148.526(15) Å^3 (1149.757(15) Å^3), $R_{wp} = 4.10\%$ (3.91%), $R_p = 3.30\%$ (3.18%), $R(F^2) = 3.68\%$ (3.39%), $\chi^2 = 1.23(1.10)$.
*$U_{11} = 0.0260(4)$ Å^2, $U_{22} = U_{33} = 0.0185(3)$ Å^2, $U_{12} = U_{13} = 0$, $U_{23} = 0.0043(4)$ Å^2.
**$U_{11} = 0.0287(4)$ Å^2, $U_{22} = U_{33} = 0.0215(2)$ Å^2, $U_{12} = U_{13} = 0$, $U_{23} = 0.0060(4)$ Å^2.

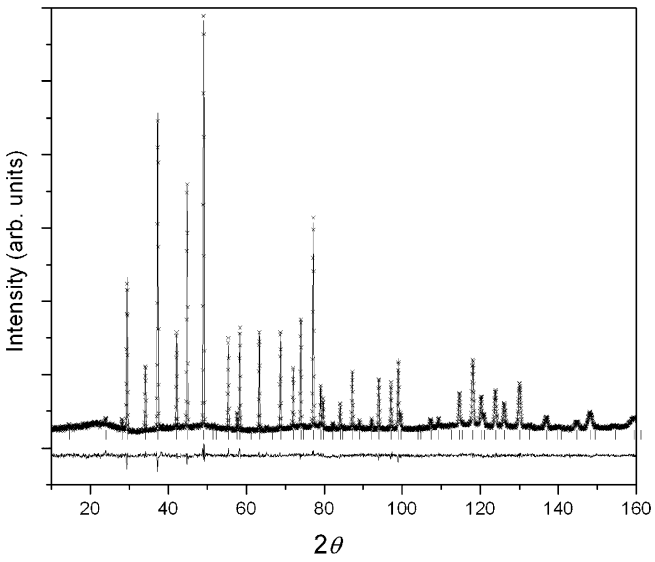

Fig. 3. Observed, calculated, and difference neutron diffraction profiles for the pyrochlore 0.4000:0.3000:0.3000 Bi_2O_3:$Mn_2O_{3\pm x}$:Nb_2O_5 at ambient temperature. Tick marks indicate allowed reflection positions.

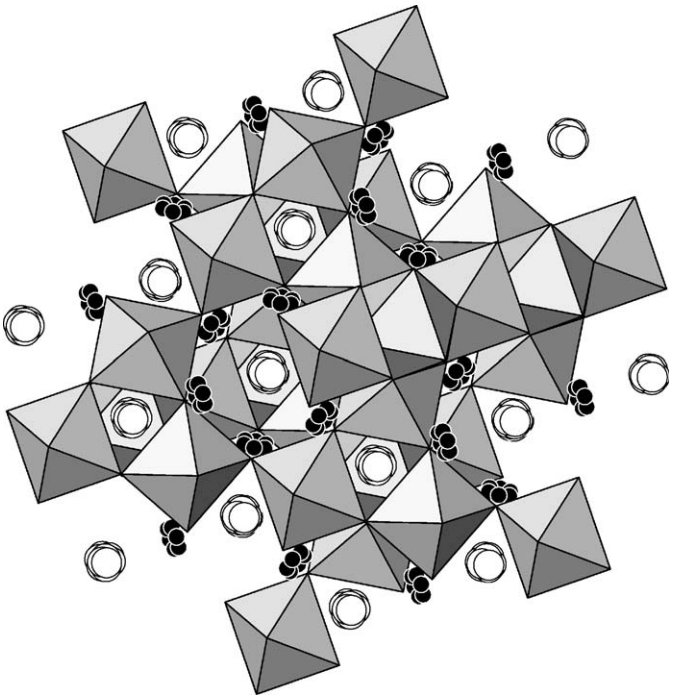

Fig. 4. Crystal structure of the pyrochlore $Bi_{1.6}Mn^{2+}_{0.4}(Mn^{3+}_{0.8}Nb_{1.2})O_7$ (Table 4) illustrating the displacive disorder of the A_2O' network. The vertex-linked polyhedra represent the octahedral $B_2O_6 = (Mn, Nb)_2O_6$ network. The toroids of black spheres represent the six equivalent 96g sites for the A-site Bi/Mn cations, and the cuboctahedral clusters of larger lighter spheres denote the 12 possible displaced positions for the O′ oxygens. The final refinement results at 12 K indicate that the A-site cations are displaced 0.361(6) Å from the ideal 16d position, while O′ is displaced 0.33(2) Å from the high-symmetry 8b position.

(0.083), suggesting the presence of few or no O′ vacancies. The refinement results are consistent with a structural formula of $Bi_{1.6}Mn^{2+}_{0.4}(Mn^{3+}_{0.8}Nb_{1.2})O_7$ for this pyrochlore, with both the A- and B-sites completely filled and with 20% of the A-sites occupied by Mn^{2+}. The displacively disordered crystal structure is illustrated in Fig. 4. The [(Mn,Nb)O_6] octahedra in the B_2O_6 network are nearly regular, with metal-oxygen distances of 2.009 Å (x6), and O–B–O angles deviating about 3.1° from 90°. The observed bond valence sum of 4.0 v.u. for the B site, calculated using the R_o parameters for Nb^{5+} and Mn^{3+} [69] and the occupancies in Table 4, is in reasonable agreement with the value of 4.2 v.u. expected from the formal valences. The A-site cations and neighboring O′ positions are both displacively disordered, therefore calculation of bond valence sums is less meaningful. However, the displaced structure results in a number of considerably shorter A–O and A–O′ distances compared to the ideal structure (Model 1): Observed A–O distances range from 2.302 to 3.023 Å (compared to 2.661 Å (x6) in the ideal structure), and observed A–O′ distances range from 2.155 to 2.459 Å (compared to 2.287 Å (x2) in the ideal structure). The shorter distances available in the displaced structure can reasonably accommodate the smaller Mn^{2+} and can also

improve the bonding for Bi^{3+} (which would have a bond valence sum of 2.5 v.u. in the ideal structure).

The structural model for $Bi_{1.6}Mn^{2+}_{0.4}(Mn^{3+}_{0.8}Nb_{1.2})O_7$ (Table 4) is crystallographically analogous to that found for pyrochlore-type $Bi_{1.5}Zn_{0.92}Nb_{1.5}O_{6.92}$ [51], which has a similar concentration of B-type cations on the A-sites (21%). The displacements of the A-cations (0.36 Å) and the O′ oxygens (0.3 Å) from the ideal positions are similar, albeit slightly smaller than those in the Zn analog (0.39 and 0.46 Å, respectively). In refinements of the analogous Bi–Fe–Nb–O [52] and Bi–Co–Nb–O [53] pyrochlores, the A-site cations were also displaced to the 96g sites but O′ was displaced differently in each case—possibly a result of different concentrations of B-type ions on the A-sites (<10% and ~18%, respectively). The presence of smaller B-type cations on the A-sites should drive distortions to reduce their effective coordination number and achieve chemically reasonable bond distances; therefore, correlations between A-site occupancies and the details of the O′ displacements are expected.

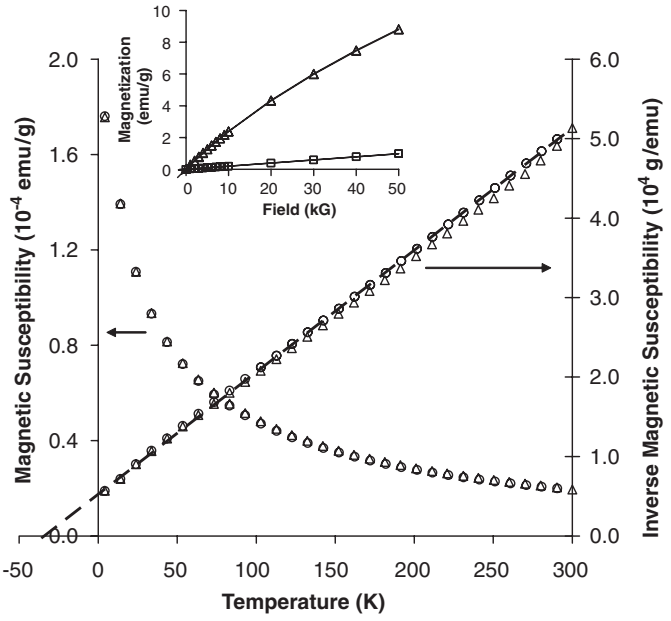

Fig. 5. Temperature dependence of the zero-field-cooled (circles) and field-cooled (triangles) mass susceptibility and inverse mass susceptibility for the pyrochlore 0.3600:0.3200:0.3200 Bi_2O_3:$Mn_2O_{3\pm x}$:Nb_2O_5 at an applied field of 50 kG. Similar results were obtained with an applied field of 20 kG. The inset shows the field dependence of the magnetization measured at 4.2 K (triangles) and 300 K (squares). (Lines are present to guide the eye.) The slight curvature observed in the low-temperature data suggests the presence of weak superparamagnetic effects. (*Units*: To convert susceptibility values in emu/g to SI units m^3/kg, multiply by $4\pi/10^3$ To convert field values in Oe (or G) to SI units A/m, multiply by $10^3/4\pi$. Magnetization values in emu/g units are numerically equal to SI units of A m^2/kg [70]).

3.4. Magnetic properties of pyrochlore phases

Magnetic data obtained for three different single-phase Bi–Mn–Nb–O pyrochlore samples indicated qualitatively similar properties. The field dependence of the magnetization confirmed that all samples were overall paramagnetic in nature. The temperature dependence of the magnetic susceptibility, and its inverse, for the pyrochlore with composition 0.3600:0.3200:0.3200 Bi_2O_3:$Mn_2O_{3\pm x}$:Nb_2O_5 are shown in Fig. 5. Above 100 K the inverse magnetic susceptibility was linear and that range was used to fit the Curie–Weiss law; the results are given in Table 5. For all three compounds, the extrapolation of the linear fits indicated small negative temperature intercepts, suggesting the presence of weak antiferromagnetic cooperative interactions. All of the observed effective magnetic moments calculated from the slopes of the Curie–Weiss fits are depressed relative to the spin-only values expected for a mixture of A-site Mn^{2+} ($3d^5$, high spin $S = 5/2$, 5.92 μ_B) and B-site Mn^{3+} ($3d^4$, high spin $S = 2$, 4.90 μ_B). The slight curvature observed in the magnetization vs. field data at 4.2 K (Fig. 5, inset) suggests the presence of some superparamagnetic effects. The complex magnetic behavior exhibited by the Bi–Mn–Nb–O pyrochlores is not unexpected given the triangular symmetry of the metal lattices which results in geometric magnetic frustration [71,72]. Pyrochlore compounds are known to exhibit a wide range of cooperative magnetic properties and, for example, are of significant interest as 'spin-ice' systems [73–75]. The reported magnetic behavior of the rhombohedrally distorted pyrochlore $Mn_2Sb_2O_7$ [67], with Mn^{2+} filling the A-sites, is similar to that of the Bi–Mn–Nb–O pyrochlore studied here. $Mn_2Sb_2O_7$ exhibited paramagnetic behavior that obeyed the Curie–Weiss Law which extrapolated to a small negative temperature intercept (−33 K), and indicated a somewhat depressed effective moment (5.76 μ_B)

Table 5
Magnetic data for single-phase Bi–Mn–Nb–O pyrochlore specimens

Bi_2O_3:$Mn_2O_{3\pm x}$:Nb_2O_5	Formula	μ_{eff}/mol Mn (μ_B)	θ (K)	μ_{calc}/mol Mn (μ_B)
0.3600:0.3200:0.3200	$Bi_{1.440}Mn^{2+}_{0.560}Mn^{3+}_{0.720}Nb_{1.280}O_7$	4.94	−34	5.37
0.4000:0.3000:0.3000	$Bi_{1.600}Mn^{2+}_{0.400}Mn^{3+}_{0.800}Nb_{1.200}O_7$	4.95	−35	5.26
0.4200:0.2900:0.2900	$Bi_{1.680}Mn^{2+}_{0.320}Mn^{3+}_{0.840}Nb_{1.160}O_7$	4.90	−31	5.20

The effective moments (μ_{eff}/mol Mn) and temperature-axis intercepts (θ, K) were approximated from linear fits of the inverse susceptibility data (ZFC) in the temperature range 100–300 K. The calculated spin-only moments (μ_{calc}/mol Mn) assume high-spin states for Mn^{2+} (d^5, 5.92 μ_B) occupying A-sites and Mn^{3+} (d^4, 4.90 μ_B) occupying B-sites, in proportions indicated by the formulas.

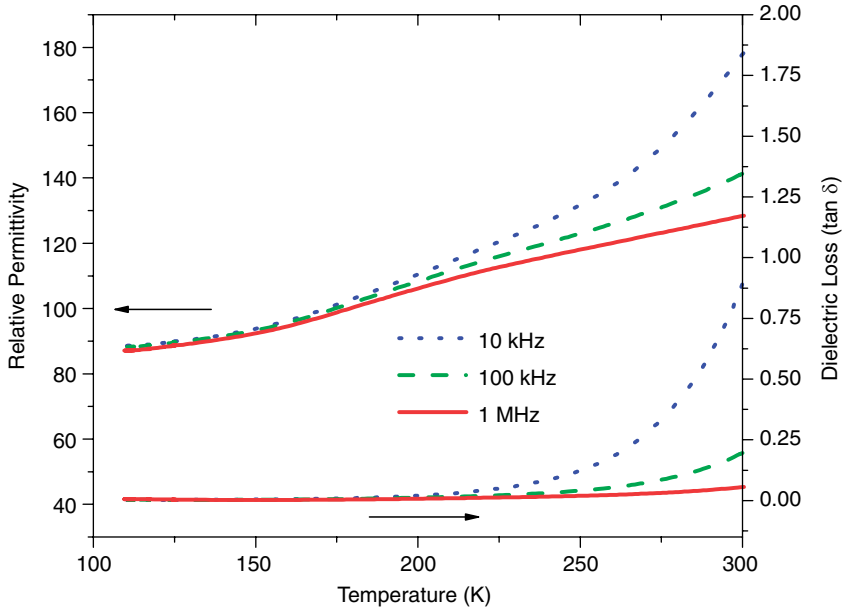

Fig. 6. Relative dielectric permittivity (corrected for porosity) and dielectric loss for the single-phase pyrochlore $Bi_{1.600}Mn_{1.200}Nb_{1.200}O_7$ (0.4000:0.3000:0.3000 Bi_2O_3:$Mn_2O_{3\pm x}$:Nb_2O_5) at frequencies of 10, 100 kHz, and 1 MHz. The sample is predominantly conductive at temperatures above 250 K and the onset of conductivity is frequency dependent; these effects likely reflect the presence of mixed-valent $Mn^{2+/3+}$. Low-temperature dielectric relaxation such as that observed for $Bi_{1.5}Zn_{0.92}Nb_{1.5}O_{6.92}$ and other bismuth-based pyrochlores was not observed.

compared to the spin-only (high-spin) value for Mn^{2+} (5.92 μ_B).

3.5. Dielectric properties of the pyrochlore phase

The relative permittivity (corrected for porosity) and dielectric loss for the single-phase pyrochlore $Bi_{1.600}Mn_{1.200}Nb_{1.200}O_7$ (0.4000:0.3000:0.3000 Bi_2O_3:$Mn_2O_{3\pm x}$:Nb_2O_5) as a function of temperature and frequency are shown in Fig. 6. The sample is predominantly conductive at temperatures above 250 K and the onset of conductivity is frequency dependent. At 300 K and 1 MHz the sample remains insulating and exhibits a relative permittivity of $\approx$128 with tan $\delta = 0.05$; however, at 10 kHz tan δ is greater than 0.8, indicating conductivity. This behavior is markedly different from that of the analogous Bi–Zn–Nb–O [76,77] and Bi–Fe–Nb–O [52] pyrochlores, which exhibit dielectric relaxation below 200 K, and likely reflects the presence of mixed-valent $Mn^{2+/3+}$. The temperature- and frequency-dependent behavior observed is consistent with interfacial polarization mediated by the multivalent Mn ions. Further experiments (e.g., impedance spectroscopy) would be required to confirm an electron hopping or related mechanism as the source of the conductive behavior.

4. Conclusions

Subsolidus phase relations have been determined for the Bi–Mn–Nb–O system in air using specimens equilibrated at 750–900 °C. Under these conditions, compounds containing Mn in the 2+, 3+, and 4+ oxidation states were all observed. Ternary phase formation was limited to pyrochlore, which forms a considerable solid solution region at stoichiometries that are "Bi-deficient" compared to conventional $A_2B_2O_7$-type formulations with Bi on the A-sites and Mn/Nb on the B-sites. The location of the pyrochlore field suggests that approximately 14–30% of the A-sites can be occupied by Mn (likely Mn^{2+}); analysis of EELS spectra indicated that the oxidation state of Mn in pyrochlore is between 2+ and 3+. All Bi–Mn–Nb–O pyrochlores form with structural displacements, as also found for analogous Bi–M–Nb–O pyrochlores with M = Zn, Fe, and Co. A structural refinement of the pyrochlore 0.4000:0.3000:0.3000 Bi_2O_3:$Mn_2O_{3\pm x}$:Nb_2O_5 using neutron powder diffraction data is reported with the displacive disorder modeled similarly to that in $Bi_{1.5}Zn_{0.92}Nb_{1.5}O_{6.92}$. The results are consistent with a structural formula of $Bi_{1.6}Mn^{2+}_{0.4}(Mn^{3+}_{0.8}Nb_{1.2})O_7$, with both the A- and B-sites completely occupied. Bi–Mn–Nb–O pyrochlores exhibited overall paramagnetic behavior with weak antiferromagnetic interactions and the presence of some superparamagnetic effects; observed moments were depressed compared to high-spin, spin-only values calculated for the corresponding $Mn^{2+/3+}$ mixtures. Measurements of relative dielectric permittivity and dielectric loss between 110 and 300 K indicated conductive, frequency-dependent properties consistent with the presence of mixed-valent Mn. In contrast to $Bi_{1.5}Zn_{0.92}Nb_{1.5}O_{6.92}$, no low-temperature dielectric relaxation was observed. Bi–Mn–Nb–O pyrochlores form thermodynamically stable mixtures with Bi_3NbO_7 solid solution, $Bi_5Nb_3O_{15}$, $BiNbO_4$, $MnNb_2O_6$,

Mn_2O_3/Mn_3O_4, and $Bi_2Mn_4O_{10}$. Crystalline, highly textured Bi–Mn–Nb–O pyrochlore films were readily deposited using pulsed laser deposition.

Acknowledgments

We thank L.P. Cook for thermogravimetric analyses, N. Swanson for graphical representation of the phase diagram data, and B. Baumgold and R.D. Shull for assistance with magnetic measurements. We appreciate helpful discussions with R.S. Roth, who also characterized single crystals. A.U. Adler was supported in part by the National Science Foundation's Research Experience for Undergraduates (REU) program, Division of Materials Research.

References

[1] N.A. Hill, A. Filippetti, J. Magn. Magn. Mater. 242 (2002) 976.
[2] A. Filippetti, N.A. Hill, Phys. Rev. B 65 (2002).
[3] N.A. Hill, J. Phys. Chem. B 104 (2000) 6694.
[4] N.A. Spaldin, M. Fiebig, Science 309 (2005) 391.
[5] W. Prellier, M.P. Singh, P. Murugavel, J. Phys.: Condens. Matter 17 (2005) R803.
[6] H. Zheng, J. Wang, S.E. Lofland, Z. Ma, L. Mohaddes-Ardabili, T. Zhao, L. Salamanca-Riba, S.R. Shinde, S.B. Ogale, F. Bai, D. Viehland, Y. Jia, D.G. Schlom, M. Wuttig, A. Roytburd, R. Ramesh, Science 303 (2004) 661.
[7] L. Fuentes, M. Garcia, J. Matutes-Aquino, D. Rios-Jara, J. Alloys Compds. 369 (2004) 10.
[8] B.H. Park, B.S. Kang, S.D. Bu, T.W. Noh, J. Lee, W. Jo, Nature 401 (1999) 682.
[9] V.E. Wood, A.E. Austin, Magnetoelectric Interaction Phenomena in Crystals, Gordon and Breach, London, 1975.
[10] P. Baettig, N.A. Spaldin, Appl. Phys. Lett. 86 (2005).
[11] D.V. Efremov, J. Van den Brink, D.I. Khomskii, Nat. Mater. 3 (2004) 853.
[12] N.A. Hill, K.M. Rabe, Phys. Rev. B 59 (1999) 8759.
[13] T. Kimura, S. Kawamoto, I. Yamada, M. Azuma, M. Takano, Y. Tokura, Phys. Rev. B 67 (2003).
[14] B.B. Van Aken, T.T.M. Palstra, A. Filippetti, N.A. Spaldin, Nat. Mater. 3 (2004) 164.
[15] M. Kenzelmann, A.B. Harris, S. Jonas, C. Broholm, J. Schefer, S.B. Kim, C.L. Zhang, S.W. Cheong, O.P. Vajk, J.W. Lynn, Phys. Rev. Lett. 95 (2005).
[16] O.P. Vajk, M. Kenzelmann, J.W. Lynn, S.B. Kim, S.W. Cheong, Phys. Rev. Lett. 94 (2005).
[17] M. Azuma, K. Takata, T. Saito, S. Ishiwata, Y. Shimakawa, M. Takano, J. Am. Chem. Soc. 127 (2005) 8889.
[18] N.A. Spaldin, W.E. Pickett, J. Solid State Chem. 176 (2003) 615.
[19] C.G. Bergeron, S.H. Risbud, Introduction to Phase Equilibria in Ceramics, American Ceramic Society, Westerville, 1984.
[20] C.S. Barrett, Structure of Metals, McGraw-Hill, New York, 1943. Vol, first ed. (Chapter X).
[21] C.R. Hubbard, Y. Zhang, R.L. McKenzie, Certificate of Analysis, SRM 660. National Institute of Standards and Technology, Gaithersburg MD, 1989.
[22] R.F. Egerton, Electron Energy Loss Spectroscopy in the Electron Microscope, Plenum Press, New York, 1996.
[23] Phase Equilibria Diagrams (formerly Phase Diagrams for Ceramists). The American Ceramic Society, Westerville, OH, 2006, Figs. 324, 327e, EC-156.
[24] U. Delicat, S.F. Radaev, M. Tromel, P. Behrens, Y.F. Kargin, A.A. Marin, J. Solid State Chem. 110 (1994) 66.
[25] A. Munoz, J.A. Alonso, M.T. Casais, M.J. Martinez-Lope, J.L. Martinez, M.T. Fernandez-Diaz, Phys. Rev. B 65 (2002).
[26] N. Nguyen, M. Legrain, A. Ducouret, B. Raveau, J. Mater. Chem. 9 (1999) 731.
[27] T. Atou, H. Chiba, K. Ohoyama, Y. Yamaguchi, Y. Syono, J. Solid State Chem. 145 (1999) 639.
[28] R. Seshadri, N.A. Hill, Chem. Mater. 13 (2001) 2892.
[29] A.M. dos Santos, A.K. Cheetham, T. Atou, Y. Syono, Y. Yamaguchi, K. Ohoyama, H. Chiba, C.N.R. Rao, Phys. Rev. B 66 (2002).
[30] H. Faqir, H. Chiba, M. Kikuchi, Y. Syono, M. Mansori, P. Satre, A. Sebaoun, J. Solid State Chem. 142 (1999) 113.
[31] R.S. Roth, J.L. Waring, J. Res. NBS 66A (6) (1962) 451.
[32] R.L. Withers, C.D. Ling, S. Schmid, Z. Kristallogr. 214 (1999) 296.
[33] C.D. Ling, R.L. Withers, S. Schmid, J.G. Thompson, J. Solid State Chem. 137 (1998) 42.
[34] M. Valant, B. Jancar, U. Pirnat, D. Suvorov, J. Eur. Ceram. Soc. 25 (2005) 2829.
[35] U. Pirnat, M. Valant, B. Jancar, D. Suvorov, Chem. Mater. 17 (2005) 5155.
[36] C.D. Ling, M. Johnson, J. Solid State Chem. 177 (2004) 1838.
[37] V.P. Sirotinkin, A.A. Bush, Russ. J. Inorg. Chem. 49 (2004) 767.
[38] M. Valant, D. Suvorov, J. Am. Ceram. Soc. 86 (2003) 939.
[39] M. Valant, D. Suvorov, J. Am. Ceram. Soc. 87 (2004) 1056.
[40] E.M. Levin, R.S. Roth, J. Res. NBS 68A (1964) 189.
[41] A.F. Wells, Structural Inorganic Chemistry, fourth ed, Clarendon Press, Oxford, 1975, p. 499.
[42] M.A. Subramanian, G. Aravamudan, G.V.S. Rao, Prog. Solid State Chem. 15 (1983) 55.
[43] T.A. Vanderah, I. Levin, M.W. Lufaso, Eur. J. Inorg. Chem. (2005) 2895.
[44] W. Somphon, V. Ting, Y. Liu, R.L. Withers, Q. Zhou, B.J. Kennedy, J. Solid State Chem. 179 (2006) 2462–2472.
[45] Ismunandar, B.J. Kennedy, B.A. Hunter, Mater. Res. Bull. 34 (1999) 1263.
[46] B.J. Kennedy, Physica B 241 (1997) 303.
[47] M. Bruhwiler, S.M. Kazakov, N.D. Zhigadlo, J. Karpinski, B. Batlogg, Phys. Rev. B 70 (2004) 020503.
[48] I.V. Piir, D.A. Prikhodko, S.V. Ignatchenko, A.V. Schukariov, Solid State Ionics 101–103 (1997) 1141.
[49] D. Ismunandar, B.J. Kennedy, B.A. Hunter, J. Alloys Compds. 302 (2000) 94.
[50] V.P. Sirotinkin, A.A. Bush, Inorg. Mater. 39 (2003) 974.
[51] I. Levin, T.G. Amos, J.C. Nino, T.A. Vanderah, C.A. Randall, M.T. Lanagan, J. Solid State Chem. 168 (2002) 69.
[52] M.W. Lufaso, T.A. Vanderah, I.M. Pazos, I. Levin, J.C. Nino, V. Provenzano, P.K. Schenck, 2006, submitted for publication.
[53] T.A. Vanderah, T. Siegrist, M.W. Lufaso, M.C. Yeager, J.C. Nino, S. Yates, Eur. J. Inorg. Chem., 2006, in press.
[54] D.M. Pease, S.D. Bader, M.B. Brodsky, J.I. Budnick, T.I. Morrison, J. Zaluzec, Phys. Lett. A. 114 (1986) 491.
[55] D.H. Pearson, C.C. Ahn, B. Fultz, Phys. Rev. B 47 (1993) 8471.
[56] Z.L. Wang, J.S. Yin, Y.D. Jiang, Micron 31 (2000) 571.
[57] M. Avdeev, M.K. Haas, J.D. Jorgensen, R.J. Cava, J. Solid State Chem. 169 (2002) 24.
[58] T. Birchall, A.W. Sleight, J. Solid State Chem. 13 (1975) 118.
[59] J.L. Fourquet, H. Duroy, P. Lacorre, J. Solid State Chem. 114 (1995) 575.
[60] M. Ganne, K. Toyama, Mater. Res. Bull. 10 (1975) 1313.
[61] A.L. Hector, S.B. Wiggin, J. Solid State Chem. 177 (2004) 139.
[62] X. Ismunandar, T. Kamiyama, K. Oikawa, A. Hoshikawa, B.J. Kennedy, Y. Kubota, K. Kato, Mater. Res. Bull. 39 (2004) 553.
[63] R.H. Jones, K.S. Knight, J. Chem. Soc.—Dalton Trans. (1997) 2551.
[64] B.J. Kennedy, Ismunandar, M.M. Elcombe, Mater. Sci. Forum 278 (2) (1998) 762.
[65] S. Uma, S. Kodialam, A. Yokochi, N. Khosrovani, M.A. Subramanian, A.W. Sleight, J. Solid State Chem. 155 (2000) 225.
[66] R.L. Withers, T.R. Welberry, A.K. Larsson, Y. Liu, L. Noren, H. Rundlof, F.J. Brink, J. Solid State Chem. 177 (2004) 231.

[67] M.A. Subramanian, A. Clearfield, A.M. Umarji, G.K. Shenoy, G.V.S. Rao, J. Solid State Chem. 52 (1984) 124.
[68] P.G. Casado, J.A. Alonso, J.L. Martinez, M.T. Fernandez, I. Rasines, Chem. Mater. 12 (2000) 1217.
[69] N.E. Brese, M. O'Keeffe, Acta Crystallogr. B 47 (1991) 192–197 with updated Ro parameters 〈http://www.ccp14.ac.uk/ccp/web-mirrors/i_d_brown/〉.
[70] R.B. Goldfarb, in: J. Evetts (Ed.), Concise Encyclopedia of Superconducting and Magnetic Materials, Pergamon Press, Oxford, 1992, p. 256.
[71] J.E. Greedan, J. Mater. Chem. 11 (2001) 37.
[72] K. Ramesha, L. Sebastian, B. Eichhorn, J. Gopalakrishnan, J. Mater. Chem. 13 (2003) 2011.
[73] A.P. Ramirez, A. Hayashi, R.J. Cava, R. Siddharthan, B.S. Shastry, Nature 399 (1999) 333.
[74] R. Siddharthan, B.S. Shastry, A.P. Ramirez, A. Hayashi, R.J. Cava, S. Rosenkranz, Phys. Rev. Lett. 83 (1999) 1854.
[75] G.D. Blundred, C.A. Bridges, M.J. Rosseinsky, Ang. Chem.-Int. Ed. 43 (2004) 3562.
[76] J.C. Nino, M.T. Lanagan, C.A. Randall, J. Appl. Phys. 89 (2001) 4512.
[77] J.C. Nino, H.J. Youn, M.T. Lanagan, C.A. Randall, J. Mater. Res. 17 (2002) 1178.